AGU PUBLICATIONS

JGR

Journal of Geophysical Research: Atmospheres

RESEARCH ARTICLE
10.1002/2016JD025561

Key Points:
- BrO observations throughout the tropics from 1 to 15 km were typically below a limit of detection of 1 pptv and were compatible with zero
- BrO and HOBr were observed at significant levels in biomass burning plumes in the tropical free troposphere
- Model calculations indicate that BrO is a minor constituent of Br_y in the tropics and highlight the importance of measuring HBr in the future

Supporting Information:
- Supporting Information S1

Correspondence to:
L. G. Huey,
greg.huey@eas.gatech.edu

Citation:
Chen, D., et al. (2016), Airborne measurements of BrO and the sum of HOBr and Br_2 over the Tropical West Pacific from 1 to 15 km during the CONvective TRansport of Active Species in the Tropics (CONTRAST) experiment, *J. Geophys. Res. Atmos.*, *121*, 12,560–12,578, doi:10.1002/2016JD025561.

Received 22 JUN 2016
Accepted 11 OCT 2016
Accepted article online 13 OCT 2016
Published online 31 OCT 2016

Airborne measurements of BrO and the sum of HOBr and Br_2 over the Tropical West Pacific from 1 to 15 km during the CONvective TRansport of Active Species in the Tropics (CONTRAST) experiment

Dexian Chen[1], L. Gregory Huey[1], David J. Tanner[1], Ross J. Salawitch[2,3,4], Daniel C. Anderson[2], Pamela A. Wales[3], Laura L. Pan[5], Elliot L. Atlas[6], Rebecca S. Hornbrook[5], Eric C. Apel[5], Nicola J. Blake[7], Teresa L. Campos[5], Valeria Donets[6], Frank M. Flocke[5], Samuel R. Hall[5], Thomas F. Hanisco[8], Alan J. Hills[5], Shawn B. Honomichl[5], Jørgen B. Jensen[5], Lisa Kaser[5], Denise D. Montzka[5], Julie M. Nicely[3,8], J. Michael Reeves[5], Daniel D. Riemer[6], Sue M. Schauffler[5], Kirk Ullmann[5], Andrew J. Weinheimer[5], and Glenn M. Wolfe[8,9]

[1]School of Earth & Atmospheric Sciences, Georgia Tech, Atlanta, Georgia, USA, [2]Department of Atmospheric and Oceanic Science, University of Maryland, College Park, Maryland, USA, [3]Department of Chemistry and Biochemistry, University of Maryland, College Park, Maryland, USA, [4]Earth System Science Interdisciplinary Center, University of Maryland, College Park, Maryland, USA, [5]National Center for Atmospheric Research, Boulder, Colorado, USA, [6]Rosenstiel School of Marine and Atmospheric Chemistry, University of Miami, Coral Gables, Florida, USA, [7]Department of Chemistry, University of California, Irvine, California, USA, [8]Atmospheric Chemistry and Dynamics Laboratory, NASA Goddard Space Flight Center, Greenbelt, Maryland, USA, [9]Joint Center for Earth Systems Technology, University of Maryland, Baltimore County, Maryland, USA

Abstract A chemical ionization mass spectrometer was used to measure BrO and HOBr + Br_2 over the Tropical West Pacific Ocean within the altitude range of 1 to 15 km, during the CONvective TRansport of Active Species in the Tropics (CONTRAST) campaign in 2014. Isolated episodes of elevated BrO (up to 6.6 pptv) and/or HOBr + Br_2 (up to 7.3 pptv) were observed in the tropical free troposphere (TFT) and were associated with biomass burning. However, most of the time we did not observe significant BrO or HOBr + Br_2 in the TFT and the tropical tropopause layer (TTL) above our limits of detection (LOD). The 1 min average LOD for BrO ranged from 0.6 to 1.6 pptv and for HOBr + Br_2 ranged from 1.3 to 3.5 pptv. During one flight, BrO observations from the TTL to the extratropical lowermost stratosphere were used to infer a profile of inorganic bromine (Br_y). Based on this profile, we estimated the product gas injection of bromine species into the stratosphere to be 2 pptv. Analysis of Br_y partitioning further indicates that BrO levels are likely very low in the TFT environment and that future studies should target the measurement of HBr or atomic Br.

1. Introduction

Bromine compounds are important ozone-depleting substances [e.g., *Daniel et al.*, 1999; *World Meteorological Organization (WMO)*, 2011, 2014; *Wennberg et al.*, 1994; *Salawitch et al.*, 2005]. Ozone (O_3) is destroyed much more efficiently by bromine, than by chlorine [e.g., *Daniel et al.*, 1999; *Danilin et al.*, 1996]. Current estimates of the stratosphere bromine loading range from 16 to 23 pptv, which is roughly 150 times lower than stratospheric chlorine [*Carpenter et al.*, 2014]. However, bromine accounts for 20 to 40% of the ozone (O_3) loss in the lowermost stratosphere (LMS) at midlatitudes [*Lee et al.*, 2002] and ~50% of the O_3 loss in the Antarctic ozone hole [e.g., *Lee et al.*, 2002; *Danilin et al.*, 1996; *Frieler et al.*, 2006; *Salawitch et al.*, 1993]. Consequently, even low concentrations of bromine have a relatively large impact on O_3 [*Salawitch et al.*, 2005].

Bromine is supplied to the stratosphere by three routes. First, the long-lived compounds methyl bromide (CH_3Br) and halons cross the tropopause, typically without decomposing. This process has been studied for a long time and the stratospheric supply of bromine from CH_3Br and halons is well understood [*Carpenter et al.*, 2014]. Methyl bromide has both natural and anthropogenic sources; the present atmospheric loading is dominated by natural sources, due to the success of the Montreal Protocol. Halons (banned by the Montreal Protocol) have only anthropogenic sources and are slowly declining due to long atmospheric lifetimes. The other two routes for supply of bromine to the stratosphere involve very short lived (VSL) compounds produced by oceanic organisms, which can cross the tropopause either without decomposing or

Table 1. The Partitioning of Br_y

	Reaction
(R1)	$Br + O_3 \rightarrow BrO + O_2$
(R2a)	$BrO + BrO \rightarrow Br_2 + O_2$
(R2b)	$BrO + BrO \rightarrow Br + Br + O_2$
(R3)	$BrO + h\upsilon \rightarrow Br + O(^3P)$
(R4)	$BrO + HO_2 \rightarrow HOBr + O_2$
(R5)	$BrO + OH \rightarrow Br + HO_2$
(R6)	$BrO + NO_2 + M \rightarrow BrNO_3 + M$
(R7)	$BrO + NO \rightarrow Br + NO_2$
(R8a)	$BrO + ClO \rightarrow Br + Cl + O_2$
(R8b)	$BrO + ClO \rightarrow Br + OClO$
(R8c)	$BrO + ClO \rightarrow BrCl + O_2$
(R9)	$Br + CH_2O \rightarrow HBr + HCO$
(R10)	$Br + CH_3CHO \rightarrow HBr + CH_3CO$
(R11)	$Br + HO_2 \rightarrow HBr + O_2$
(R12)	$Br_2 + h\upsilon \rightarrow Br + Br$
(R13)	$HOBr + h\upsilon \rightarrow Br + OH$
(R14a)	$BrNO_3 + h\upsilon \rightarrow Br + NO_3$
(R14b)	$BrNO_3 + h\upsilon \rightarrow BrO + NO_2$
(R15)	$BrCl + h\upsilon \rightarrow Br + Cl$
(R16)	$HBr + OH \rightarrow Br + H_2O$
(R17)	$HBr(g) \rightarrow HBr(particle)$
(R18)	$HOBr(g) \rightarrow HOBr(particle)$
(R19)	$BrNO_3(g) \rightarrow BrNO_3(particle)$
(R20)	$BrNO_3 + H_2O \xrightarrow{heterogeneous} HOBr + HNO_3$
(R21)	$HOBr + HBr \xrightarrow{heterogeneous} Br_2 + H_2O$
(R22)	$HOBr + HCl \xrightarrow{heterogeneous} BrCl + H_2O$
(R23)	$HOCl + HBr \xrightarrow{heterogeneous} BrCl + H_2O$

after decomposing in the troposphere. The term CBr_y^{VSL} refers to bromocarbons with tropospheric lifetimes less than half a year (e.g., $CHBr_3$ and CH_2Br_2), which are primarily produced by marine algae [e.g., *Ko et al.*, 2002; *Tegtmeier et al.*, 2012; *Warwick et al.*, 2006].

The input of inorganic bromine (collectively known as Br_y, $Br_y = Br + BrO + HOBr + BrNO_3 + 2 \times Br_2 + BrCl + HBr$), following the tropospheric decomposition of VSL compounds, is estimated to contribute 1.1 to 4.3 pptv to the stratospheric bromine burden [*Carpenter et al.*, 2014; *Montzka et al.*, 2011]. The input of Br_y to the stratosphere is usually termed product gas injection (PGI) of bromine species and the input of bromocarbons (CBr_y) to the stratosphere is termed source gas injection (SGI) of bromine species. The most important PGI pathway is thought to be in the tropics; the Western Pacific plays a particularly important role due to the deep convection in this region [e.g., *Pan et al.*, 2016]. Deep convection transports Br_y from the marine boundary layer (MBL) and tropical free troposphere (TFT) (1 to 12 km) to the tropical tropopause layer (TTL) (~12 to 17 km) and subsequently to the LMS [*Aschmann et al.*, 2009; *Ashfold et al.*, 2012; *Fernandez et al.*, 2014; *Levine et al.*, 2007; *Tegtmeier et al.*, 2012; *Sinnhuber and Folkins*, 2006]. The release of Br_y from saline aerosols in the lower part of the troposphere and the degradation of very short lived bromocarbons (CBr_y^{VSL}) throughout the troposphere and the TTL serve as sources of Br_y [e.g., *Ko et al.*, 1997; *Orlando*, 2003; *Yang et al.*, 2005; *Salawitch*, 2006; *Hossaini et al.*, 2010].

The computed transport of Br_y to the stratosphere is also sensitive to model treatment of the partitioning of Br_y (Table 1) [e.g., *Parrella et al.*, 2012; *Fernandez et al.*, 2014]. This sensitivity occurs because (1) soluble species such as HOBr, $BrNO_3$, and HBr are subject to loss from the gas phase by scavenging (Table 1, (R17)–(R19)) in the troposphere before being delivered to the stratosphere and (2) heterogeneous chemistry can recycle Br_y back to the gas phase (Table 1, (R20)–(R23)) and thus partially compensate for the impact of scavenging [*Iraci et al.*, 2005; *Fernandez et al.*, 2014]. For these reasons, the mechanism for PGI of Br_y is complex as it couples biological, chemical, and dynamical processes. Measurements of Br_y in the tropical troposphere are necessary to understand the whole PGI mechanism: the release of Br_y, the transport, the chemistry, and finally the amount of Br_y delivered to the stratosphere.

There has been considerable effort to measure tropospheric Br_y, mainly in the extratropical troposphere [*Choi et al.*, 2012; *Dibb et al.*, 2010; *Fitzenberger et al.*, 2000; *Hebestreit et al.*, 1999; *Hönninger et al.*, 2004; *Liao et al.*, 2011a, 2011b, 2012; *Mahajan et al.*, 2009; *Neuman et al.*, 2010; *Pommier et al.*, 2012; *van Roozendael et al.*, 2002; *Schofield et al.*, 2004]. But neither the distribution nor the partitioning of Br_y is zonally uniform in the troposphere [e.g., *von Glasow et al.*, 2004; *Yang et al.*, 2005]. To date, limited measurements in the tropical troposphere have solely focused on BrO and have led to an uncertain picture. Retrieval of BrO from the Scanning Imaging Absorption Spectrometer for Atmospheric Chartography (SCIAMACHY) satellite

Table 2. Measurements of Species and Meteorological Parameters Relevant to This Study

Instruments	Measured Species/Parameters	PI/Institutions
CIMS	BrO, HOBr + Br_2, N_2O_5	Huey/GA Tech
Chemiluminescence	O_3	Weinheimer/NCAR
Chemiluminescence	NO, NO_2	Weinheimer/NCAR
Vacuum UV Fluorescence	CO	Campos/NCAR
Picarro WS-CRDS[a]	CH_4, CO_2	Campos/NCAR
TOGA[b]	VOCs/bromocarbons/HCN	Apel/NCAR & Riemer/U Miami
AWAS[c]	VOCs/bromocarbons	Atlas/U Miami
ISAF[d]	CH_2O	Hanisco/NASA
HARP[e]	actinic flux	Hall/NCAR
VCSEL[f]	H_2O vapor	Jensen/NCAR
2DC[g]	cloud droplets (12.5–3200 μm)	Jensen/NCAR
CDP[h]	particle (2–50 μm)	Jensen/NCAR
UHSAS[i]	particle (0.06–1 μm)	Jensen/NCAR
GV platform	time, location, *T*, *p*, Wind	Jensen/NCAR

[a]Wavelength-scanned cavity ring-down spectroscopy.
[b]Trace organic gas analyzer.
[c]Advance whole air sampler.
[d]In situ airborne formaldehyde.
[e]HIAPER airborne radiation package.
[f]Vertical cavity surface emitting laser hygrometer.
[g]Two-dimensional optical array cloud probe.
[h]Cloud droplet probe.
[i]Ultrahigh sensitivity aerosol spectrometer.

instrument suggested that the BrO column below 15 km across the equator is equivalent to a uniform distribution of 1 pptv BrO throughout the tropospheric column [*Sinnhuber et al.*, 2005]. On the other hand, SCIAMACHY BrO retrieved in other work suggested the presence of 2 to 4 pptv of BrO in the tropical upper troposphere, with little or no BrO present below 15 km [*Sioris et al.*, 2006]. *Theys et al.* [2007] deduced a maximum 2 to 5 pptv of BrO in the free troposphere above Réunion Island (21°S, 56°E) according to the measured vertical tropospheric BrO column, $(1.1 \pm 0.45) \times 10^{13}$ molecule $\cdot$ cm^{-2}, by a differential optical absorption spectroscopy (DOAS). In contrast, another DOAS instrument performed measurements in Teresina, Brazil (5.1°S, 42.9°W), and it was concluded that BrO in the TFT is compatible with zero with the uncertainties of around 1 pptv [*Dorf et al.*, 2008]. In addition, the model simulation by *von Glasow et al.* [2004] suggested that an unknown source of Br_y would need to be assumed in the TFT to explain higher levels of observed BrO. It has also been suggested that the partitioning of Br_y in the TFT and TTL may be shifted to species other than BrO, such as HBr, HOBr, or Br [*Fernandez et al.*, 2014; *von Glasow et al.*, 2004; *Liang et al.*, 2014; *Yang et al.*, 2005]. Thus, a small amount of BrO observed in the TFT and TTL can reflect the presence of a much higher amount of Br_y. Consequently, the full assessment of PGI requires observations of a wider suite of inorganic bromine species in the tropics.

The CONvective TRansport of Active Species in the Tropics (CONTRAST) experiment was an airborne investigation utilizing the National Center for Atmospheric Research (NCAR) Gulfstream-V (GV) aircraft equipped with a suite of chemical and meteorological parameter instruments. The CONTRAST flights were based out of Guam (13.5°N, 144.6°E) during January and February 2014. A complete description of the CONTRAST experiment is detailed in the overview paper [*Pan et al.*, 2016]. A primary scientific objective was to study the chemistry and transport of Br_y into the TTL and LMS over the Tropical West Pacific Ocean. During CONTRAST, we measured BrO as well as the sum of Br_2 and HOBr (HOBr + Br_2) using a chemical ionization mass spectrometer (CIMS). These results represent some of the first observations of Br_y species other than BrO in the tropics. Observations of both BrO and HOBr + Br_2 can provide more information for the assessment of local Br_y chemistry and PGI.

2. Measurements

A suite of instruments used during CONTRAST related to this study are listed in Table 2. The dynamical and chemical models for forecasting and flight planning are documented in the CONTRAST field catalog (http://

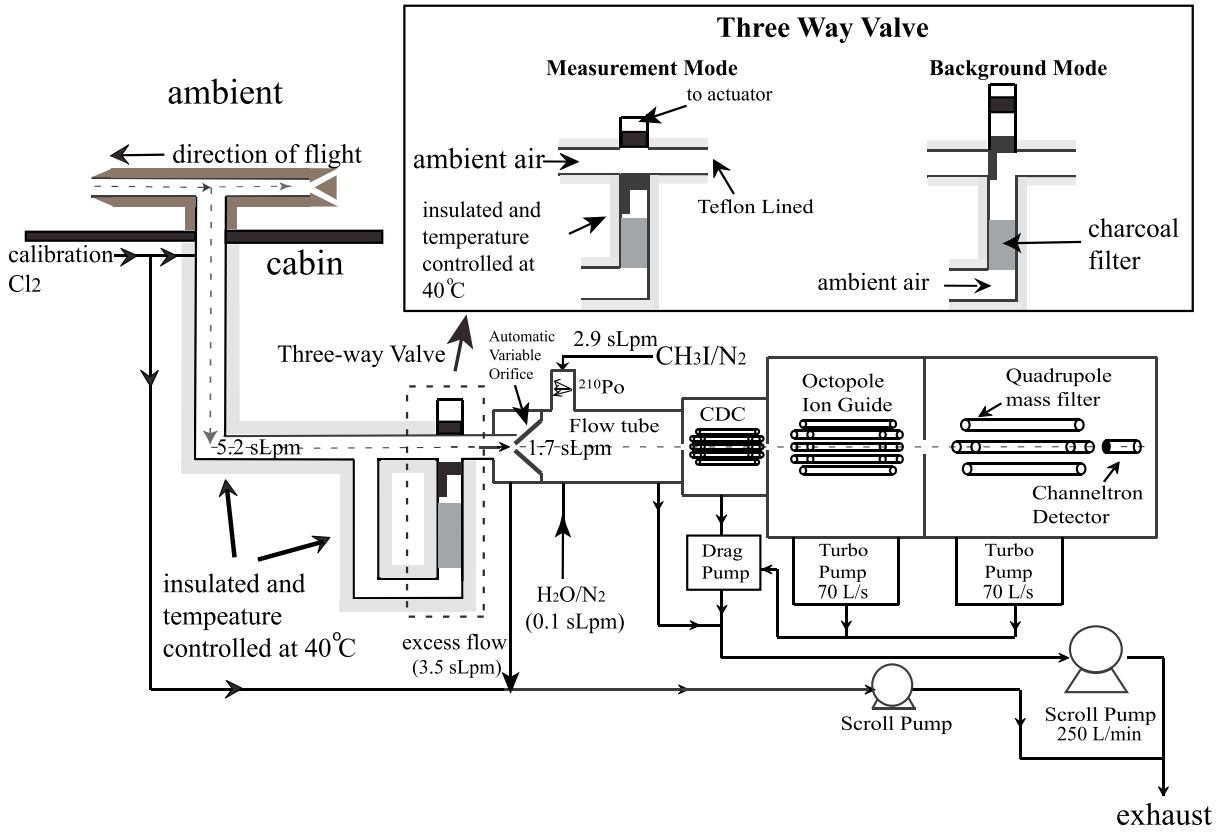

Figure 1. The configuration of CIMS used in CONTRAST, adapted from *Liao et al.* [2011a].

catalog.eol.ucar.edu/contrast) and described in *Pan et al.* [2016]. In this section, we focus on the CIMS employed for measurements of BrO and $HOBr + Br_2$.

2.1. CIMS

CIMS utilizes a reagent ion to selectively react and ionize targeted atmospheric species [*Huey*, 2007]. The CIMS instrument used in this work is very similar to that described by *Kim et al.* [2007] and *Liao et al.* [2011a]. Here we briefly describe the configuration of the CIMS used in this experiment (Figure 1) and how it differed from earlier versions. As in previous work, the CIMS was composed of the following differentially pumped regions: a flow tube, a collisional dissociation chamber (CDC), an octopole ion guide, a quadrupole mass filter, and an ion detector. These components were evacuated by a scroll pump (Varian TriScroll^{TM} 300), a drag pump (Adixen MDP 5011), and two turbo pumps (Varian Turbo-V70), respectively. Air was sampled via an orifice into the flow tube, where the ion molecule reactions took place. The ionized products were sampled into the CDC, where the collision energy between ions and neutral molecules was enhanced by an electric field. Weakly bound cluster ions (mainly water cluster ions) were dissociated into core ions (e.g., $Br_2 \cdot I^- \cdot (H_2O)_n$ was dissociated into $Br_2 \cdot I^-$). Then ionization products were guided by the octopole to the quadrupole for mass selection and then detection.

During CONTRAST, smaller turbo pumps were used to evacuate the octopole and quadrupole regions (i.e., Varian Turbo-V70 instead of Varian Turbo-V300), to reduce size, weight, and power consumption of this instrument relative to previous versions. In addition, the flow tube was elongated to ~20 cm, and the operating pressure was increased from 20 to 50 torr to maximize the sensitivity of the CIMS to BrO species. This increased the concentrations of both the reagent ion and measured species in the flow tube while also increasing reaction time. This resulted in an increase in sensitivity for BrO from ~3 $Hz \cdot pptv^{-1}$ to ~10 $Hz \cdot pptv^{-1}$.

In previous studies, we used an orifice of fixed area in the entrance to the flow tube to sample air. For an orifice of fixed area, the sample volumetric flow (in liter per minute) is constant, but the sample mass flow (in

sLpm, standard liter per minute, standard = 0°C and 1013 hPa) decreases at high altitudes as the pressure decreases, resulting in a decreasing CIMS sensitivity. In CONTRAST, to stabilize the CIMS sensitivity at higher altitudes, an automatic variable orifice (AVO) was used to maintain the sample mass flow. The area of the AVO increased as the ambient pressure decreased, keeping the flow tube pressure constant. The area of the AVO was controlled by the combination of a microprocessor and stepping motor, which moved a polished piece of stainless steel across a triangular shaped opening.

2.2. Inlet

Ambient air was delivered to the CIMS from a standard GV chemical inlet (Figure 1). The inlet probe was a cigar-shaped faring that housed a Teflon^{TM} FEP tube (outer diameter = 1.3 cm, inner diameter = 1 cm, ~1 m long). The whole inlet was maintained at 40°C to keep it warmer than ambient for all flight conditions while avoiding thermal decomposition of species such as bromine nitrate. At all altitudes, a constant flow of 5.2 sLpm was maintained in the inlet tubing, of which 3.5 sLpm was exhausted through a mass flow controller and the remaining 1.7 sLpm sampled through the AVO.

2.3. Ion Chemistry

We used hydrated iodide ion ($I^- \cdot (H_2O)_n$) as the reagent ion. $I^- \cdot (H_2O)_n$ has been utilized to selectively detect a series of halogen and nitrogen containing compounds [*Huey*, 2007; *Bertram and Thornton*, 2009; *Kercher et al.*, 2009; *Liao et al.*, 2011a, 2011b, 2012, 2014; *Neuman et al.*, 2010; *Slusher et al.*, 2004; *Zheng et al.*, 2011]. Iodide was produced by flowing 2.9 sLpm of N_2, containing a few ppmv CH_3I (99.5%, Alfa Aesar) over a ^{210}Po ion source into the flow tube. In addition, 0.1 sLpm of humidified N_2 was introduced separately into the flow tube to ensure that the iodide ion was hydrated throughout the altitude range of the aircraft. In the flow tube, targeted species were ionized via the reactions below [*Liao et al.*, 2011a, 2011b, 2012; *Neuman et al.*, 2010]:

(R24) $$I^- \cdot (H_2O)_n + BrO \rightarrow BrO \cdot I^- (m/z = 222,\ 224) + nH_2O$$

(R25) $$I^- \cdot (H_2O)_n + HOBr \rightarrow HOBr \cdot I^- (m/z = 223,\ 225) + nH_2O$$

(R26) $$I^- \cdot (H_2O)_n + Br_2 \rightarrow Br_2 \cdot I^- (m/z = 285,\ 287,\ 289) + nH_2O.$$

BrO, HOBr, and Br_2 were detected as their corresponding cluster ions with I^- ((R24)–(R26)). However, it should be noted that we express the ionization products as their core ion forms for simplicity; the water molecules in these clusters were removed in the CDC (section 2.1). Each product ion has at least two isotopes due to the presence of natural ^{79}Br (50.69%) and ^{81}Br (49.31%), and thus, the concentration of each species can be derived from signals at more than one mass. We derived concentrations for each species from all the detected masses. For each flight, we derived the concentrations from the mass peak with the least noise and/or interference levels. However, for most of the experiment we used *m/z* 222 for BrO, *m/z* 225 for HOBr, and *m/z* 287 for Br_2. It should also be pointed out that HOBr can be efficiently converted to Br_2 in the type of inlet used in this study [*Neuman et al.*, 2010]. Hence we report HOBr + Br_2 instead of HOBr and Br_2 separately, although under sunlit conditions HOBr is expected to dominate due to the short photolytic lifetime of Br_2.

2.4. Background Determination

The instrumental background was periodically determined during the research flights (RF) for 1 min out of every 10 min. A custom-made three-way Teflon^{TM} valve was used to switch between measurement mode and background mode (Figure 1). In background mode, ambient air passed through an activated carbon scrubber before being introduced into the CIMS. The scrubber was found to remove >99% of targeted species in ambient air. The three-way Teflon^{TM} valve and all tubing were also thermostatted at 40°C.

2.5. Calibrations

Since portable standards of BrO and HOBr have not yet been developed, we calibrated the CIMS indirectly. In the field, a known amount of Cl_2 gas from a permeation tube (KIN-TEK) was introduced to the inlet to measure the sensitivity in flights [*Liao et al.*, 2012, 2014].

(R27) $$I^- \cdot (H_2O)_n + Cl_2 \rightarrow Cl_2 \cdot I^- (m/z = 197,\ 199,\ 201) + nH_2O.$$

Table 3. Species Included in the Steady State Model[a]

	Species
Constrained	O_3, H_2O(v), NO, CO, CH_4, C_2H_6, CH_3OH, CH_2O, CH_3CHO, $CH_3C(O)CH_3$, BrO, HCl[b], Cl[b]
Steady state	$O(^3P)$, $O(^1D)$, OH, HO_2, CH_3O_2, $CH_3C(O)CH_2O_2$, NO_2, HOBr, Br, $BrNO_3$, BrCl, ClO

[a]For inorganic chlorine species the model only considered HCl, Cl, and ClO. The interconversions between Cl and ClO were rapid under CONTRAST conditions ($Cl + O_3 \rightarrow ClO + O_2$, $ClO + NO \rightarrow Cl + NO_2$, $ClO + h\upsilon \rightarrow Cl + O(^3P)$), and thus, ClO can be estimated assuming steady state with the constraint of Cl.
[b]Estimated. See text.

The emission rates of the permeation tube were measured throughout the campaign by a spectrophotometric method [*Wu et al.*, 1963; *Kazantseva et al.*, 2002]. After the campaign, the sensitivities of BrO, HOBr, and Br_2 relative to Cl_2 were assessed in the laboratory using methods described by *Liao et al.* [2011a, 2012]. The absolute sensitivities of BrO, HOBr, and Br_2 were obtained from their relative sensitivity to Cl_2. The calibration uncertainty (2σ) is 23% for BrO and 25% for $HOBr + Br_2$, accounting for uncertainties of the emission rate of Cl_2, and the relative sensitivities of BrO, HOBr and Br_2 to Cl_2.

2.6. Limit of Detection (LOD)

The accurate estimate of our limit of detection (LOD) is very important in this work because we were at or below the LOD for much of the mission. Commonly, we have estimated the CIMS LOD based on the standard deviation of the variation of background signals [e.g., *Liao et al.*, 2011a; *Neuman et al.*, 2006]. In this mission, we defined the LOD as 3 times the standard deviation (3σ) of the background variations and estimated average LODs for each flight (5.2 to 8.1 h long) for BrO and $HOBr + Br_2$. The LOD of $HOBr + Br_2$ combines LODs of both HOBr and Br_2 as in equation (1).

$$\mathrm{LOD}(HOBr + Br_2) = \sqrt{[\mathrm{LOD}(HOBr)]^2 + [\mathrm{LOD}(Br_2)]^2}. \quad (1)$$

However, it should also be noted that this method may under or overestimate the true LOD when background levels varied more rapidly than the time scale of the background measurements (every 10 min) or are influenced by factors such as cabin temperature. For example, in this study we have found that background levels were higher if the cabin temperature was warmer than normal. Since we derived the concentration of a species from several masses, for each period of time, the LOD was determined based on the mass used for the derivation of concentration. For all available BrO and $HOBr + Br_2$ data in CONTRAST, this method gave the 1 min-based LOD of BrO ranging between 0.6 and 1.6 pptv, with an average of 1.0 pptv, and a median of 1.1 pptv, and gave the 1 min-based LOD of $HOBr + Br_2$ ranging between 1.3 and 3.5 pptv, with an average of 2.2 pptv, and a median of 2.1 pptv. The LOD of $HOBr + Br_2$ was higher as it accounts for uncertainties of both HOBr and Br_2.

2.7. Interferences

Due to the very low levels of halogens measured during CONTRAST, we encountered several interference issues that impacted our observations. During the first several research flights Br_2 was utilized as the calibration gas to track the sensitivities of CIMS. However, we found that the Br_2 residual in the inlet could have significantly interfered with measurements of BrO, HOBr, and Br_2. For this reason, we switched the calibration gas to Cl_2 and rinsed the inlet thoroughly before RF09 (5 February). No significant interference coming from the Br_2 residual was found on later RFs nor did we see any sign of interference generated by the Cl_2 calibration. Here we reported data from RF09 to the end of the campaign.

We have also found that high O_3 levels in the LMS interfered with both $HOBr + Br_2$ and BrO measurements. Laboratory experiments showed that an unrecognized species, which does not contain bromine atoms appears at $m/z = 222$ at high O_3 levels. This species interferes with the measurement of BrO at $m/z = 222$. However, the mechanism for producing this and other interfering masses at high O_3 is not certain but may involve chemistry driven by the formation of $O_3 \cdot I^-$ and other ions associated with O_3. The interferences impacted part of the BrO and $HOBr + Br_2$ data during RF15 (24 February). For RF15, we did not report $HOBr + Br_2$ data when $O_3 > \sim 125$ ppbv and BrO data when $O_3 > \sim 480$ ppbv.

Table 4. Species Included in the Time-Dependent Model

	Species
Constrained[a]	O_3, H_2O(v), CO, CH_4, C_2H_6, CH_3OH, CH_2O, CH_3CHO, $CH_3C(O)CH_3$
Steady state	$O(^3P)$, $O(^1D)$, OH, HO_2, CH_3O_2, $CH_3C(O)CH_2O$, NO[b], NO_2[b], Cl
Time dependent	HBr, HCl
Time dependent and Steady state[c]	Br, BrO, HOBr, BrCl, $BrNO_3$, ClO, Cl_2O_2, OClO, HOCl, $ClNO_3$

[a]Constrained species are held at measured values.
[b]NO_x is held as the sum of measured NO and calculated NO_2, while the NO/NO_2 partitioning is calculated assuming stead state.
[c]These species are treated as in steady state if their (instantaneous) lifetimes are shorter than Δt (150 s) and treated as time dependent if their lifetimes are longer. Photoreactive Br_y were initialized as calculated by the steady state model. ClO, Cl_2O_2, OClO, HOCl, and $ClNO_3$ were initialized to be zero.

3. Photochemical Models

Two zero-dimensional photochemical models [*Sjostedt et al.*, 2007; *Kim et al.*, 2007; *Liao et al.*, 2011b], a steady state model and a time-dependent model, were applied in this study. Br, Br_2, BrO, HOBr, $BrNO_3$, and BrCl have much shorter lifetimes than HBr. Here we term these shorter-lived species as photoreactive Br_y. The steady state model was used to evaluate the partitioning amongst photoreactive Br_y. The time-dependent model was used to evaluate the partitioning between HBr and photoreactive Br_y.

In the steady state model, temperature (T), pressure (p), and photodissociation rates (j values) were constrained by aircraft measurements. Long-lived chemicals (lifetime longer than hours) were also constrained by measurements, while short-lived chemicals were calculated by assuming steady state, as shown in Table 3. We only considered relatively simple organics as CONTRAST was carried out in a remote and clean environment. NO_2 was calculated assuming steady state with observed NO, O_3, j_{NO2}, etc., because measurements of NO_2 at higher altitudes were likely interfered with by thermally labile NO_y such as HO_2NO_2 and $CH_3O_2NO_2$, which can decompose to NO_2 in the heated inlet [*Browne et al.*, 2011]. For photoreactive Br_y,

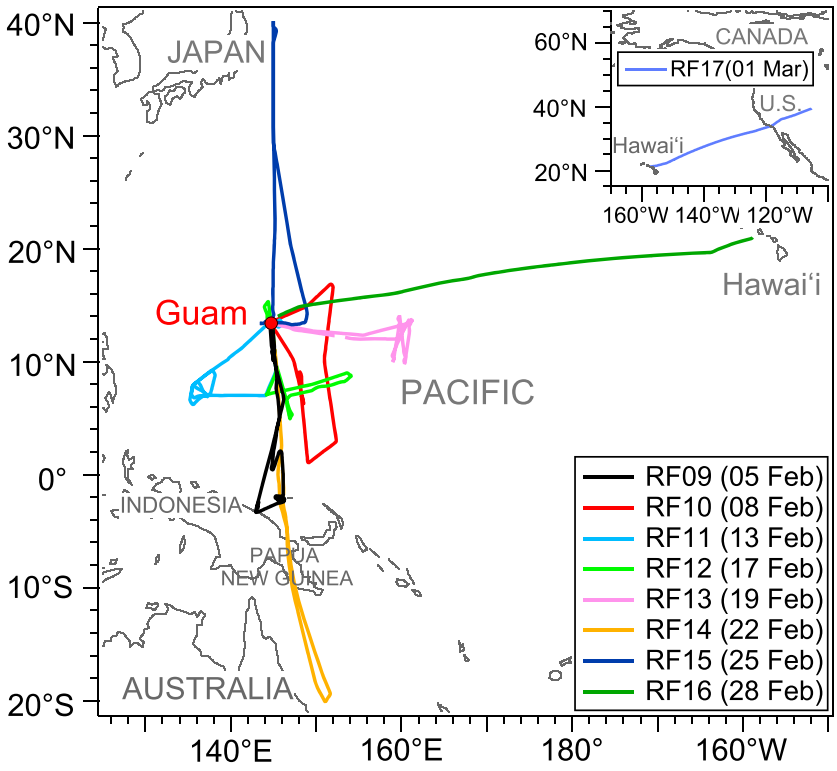

Figure 2. Flight paths during CONTRAST (RF09 to RF17).

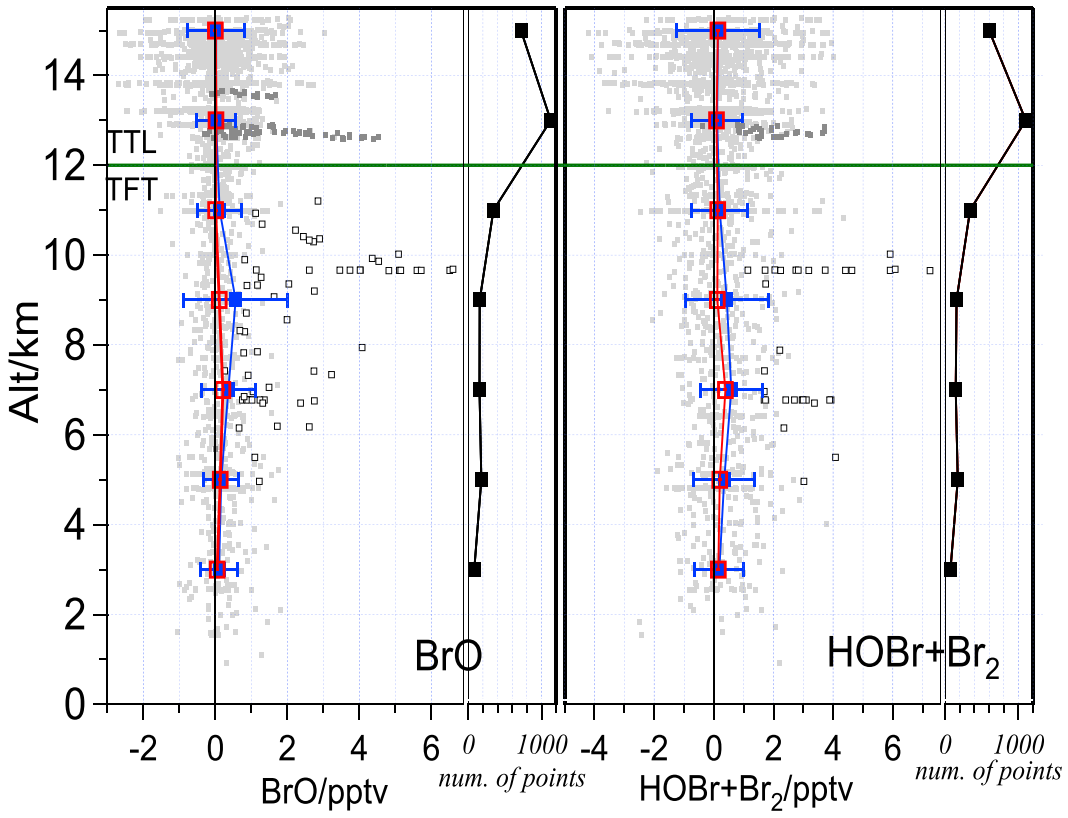

Figure 3. Vertical profiles of (left) BrO and (right) $HOBr + Br_2$. All 1 min averaged data points of BrO and $HOBr + Br_2$ are plotted. Significant BrO and $HOBr + Br_2$ levels are highlighted according to their locations: black open squares for the troposphere and black-filled squares for the TTL-LMS transition region and LMS (see section 4.4). The 2 km averages with standard deviations (blue filled squares) and medians (red open squares) of all data points in the TTL and the TFT are superposed. Significant BrO and $HOBr + Br_2$ of LMS origin are excluded when averages and medians were calculated. The numbers of data points falling into each 2 km bin are plotted on the side. Note that the medians are more representative than the averages.

BrO was constrained, and other species are calculated. We did track the ClO and BrCl masses during the campaign, but we did not observe significant signals for either compound, although the LODs for these species were relatively high (LOD(ClO) ~ 5 pptv, LOD(BrCl) ~ 2 pptv) as we did not spend much of the measurement duty cycle on these masses. To estimated BrCl, the model was constrained by estimated [Cl] and [HCl]. [Cl] was estimated in two steps: First, the [Cl] to [OH] ratio was derived from ratios of various alkanes and benzene measured by advanced whole air sampler (AWAS) and trace organic gas analyzer (TOGA) (Table 2), as described in *Rudolph et al.* [1997] and *Arsene et al.* [2007]. Then [Cl] was determined by multiplying the derived [Cl] to [OH] ratio by model calculated [OH]. [HCl] was estimated using the UWCM model (version 3) [*Wolfe and Thornton*, 2011] with the constraint of [Cl].

The time-dependent model was run with $\Delta t = 150$ s. T and p were held at observed values, while j values were parameterized as a function of solar zenith angle (SZA) and altitudes based on the data set of measured j values. Table 4 lists the chemical species and how they are treated. The time-dependent model included the heterogeneous cycling of Br_y but neglected the deposition since the time scale of deposition is much longer than of partitioning [*Parrella et al.*, 2012]. The heterogeneous reaction rate constants were calculated based on measured particle distributions. We considered background fine particles at all altitude levels and ice particles when ambient T was less than −20°C. Background fine particles were measured by ultrahigh sensitivity aerosol spectrometer (UHSAS) (Table 2). There was no specific measurement of ice particles. However, at $T < -20$°C, we assumed that particles detected by cloud particle probes (CDP and 2DC, Table 2) were ice particles. The supporting information [*Burkholder et al.*, 2015; *Crowley et al.*, 2010; *Jacob*, 2000; *Schwartz*, 1986] provides more details of both models.

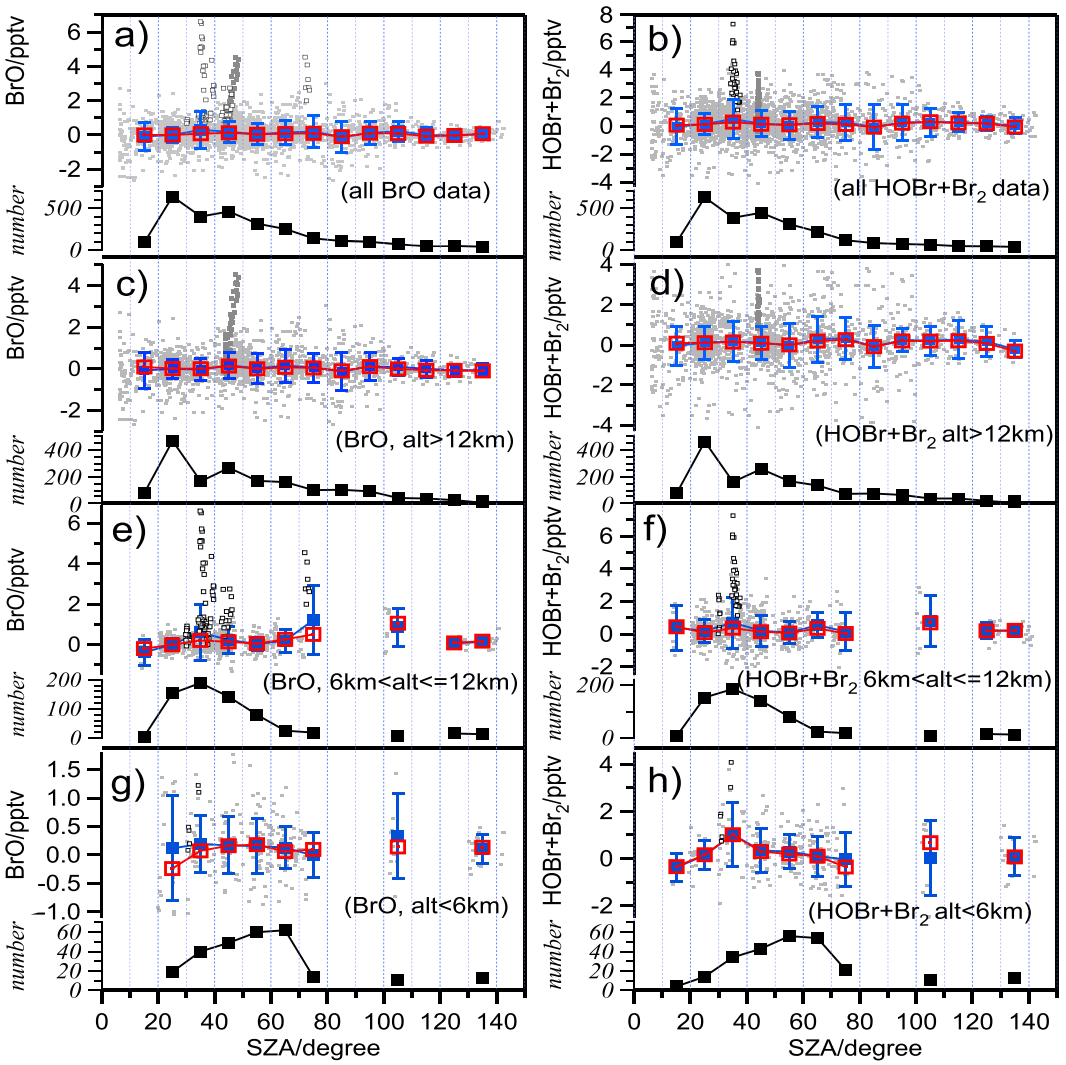

Figure 4. Diurnal profiles of BrO and HOBr + Br_2 plotted against SZA. In all panels, similar to Figure 3, all 1 min averaged data points are plotted, and significant BrO and HOBr + Br_2 are highlighted according to their locations, black open squares for troposphere, and black filled squares for the TTL-LMS transition region and LMS (see section 4.4). The 10° SZA-binned averages with standard deviation (blue filled squares), and medians (red open squares) are superposed. The numbers of data points falling into each 2 km bin are plotted on the bottom of each panel. Note that scales may be different in different panels.

4. Results

4.1. Overview

CONTRAST data are available at http://data.eol.ucar.edu/master_list/?project=CONTRAST. In this study, all analyses are based on 1 min averaged data, and all times are in UTC (Guam local time is UTC + 10 h). Flight paths for RFs 09 through 17 are shown in Figure 2. RF17 was the returning transit fight and was out of the Tropical West Pacific Ocean. Here we focus on RF09 to RF16.

From RF09 to RF16, the GV covered a wide area above the Tropical West Pacific Ocean, with an altitude range up to ~15.3 km. Sampling was mostly performed in the TTL (~32 h), with most of the remaining time in the TFT (~19 h). Observed BrO and HOBr + Br_2 in these flights are plotted against altitude in Figure 3. Most of the time we did not observe BrO or HOBr + Br_2 above the detection limit of the CIMS. However, significant levels of BrO and/or HOBr + Br_2, defined as consistently above the LOD, were observed episodically. They are highlighted in Figure 3 according to their locations (see section 4.4 for details). The averages and medians

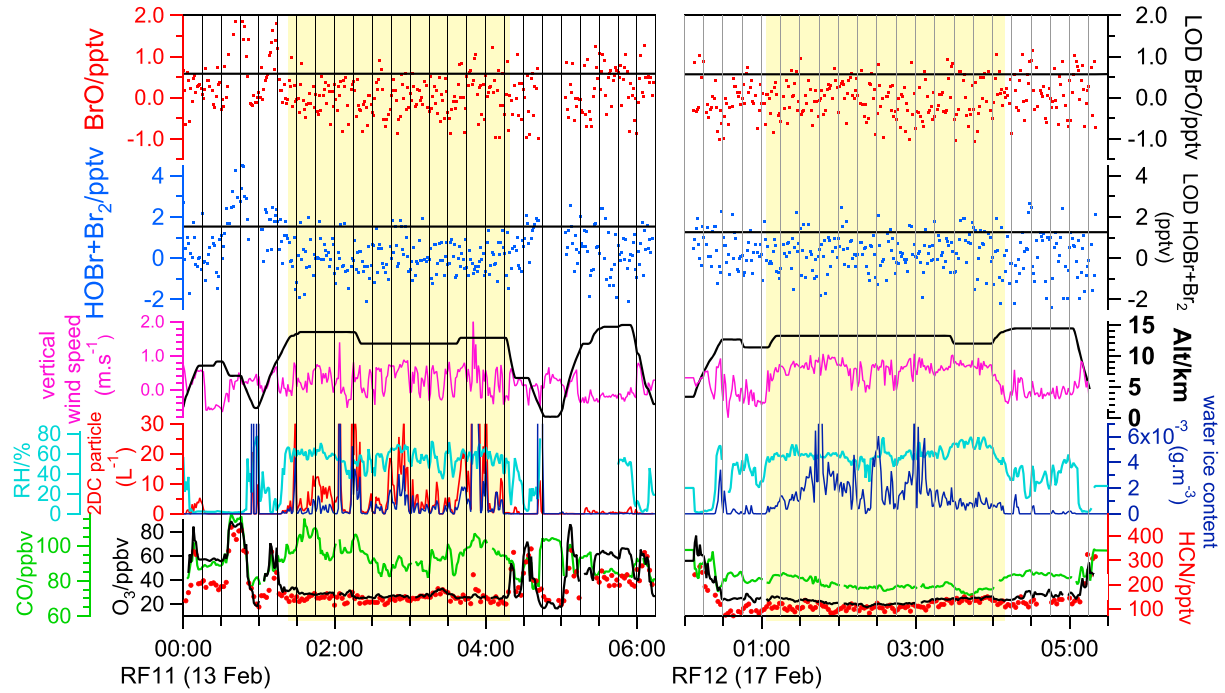

Figure 5. Time series of BrO, $HOBr + Br_2$, and related species and parameters during RF11 and RF12. Convective outflow regions are shaded in light yellow.

of BrO and $HOBr + Br_2$ based on 2 km altitude intervals are superimposed in Figure 3. The median values are probably more representative of BrO and $HOBr + Br_2$ compared to average values since episodic events can bias the averages. However, both average and median values are indistinguishable with zero within the uncertainties at all levels.

Our flights targeted both sunlit and dark conditions. The diurnal patterns of BrO and $HOBr + Br_2$ were examined by plotting them against SZA (Figure 4). Figures 4a and 4b show all data points against SZA; Figures 4c–4h show data points against SZA at three different altitude levels ($<$6 km, 6 to 12 km, and $>=$ 12 km). Similarly, averages and medians based on intervals of 10° of SZA were superposed in Figure 4a–4h. For the whole data set neither averages nor medians displayed significant departure from zero within uncertainties, and in general, the same conclusion holds for different altitude levels, especially in the TTL (altitude $>$12 km) where the sample size is relatively large. However, episodic significant levels can bias averages and medians in lower altitudes ($<$6 km, and 6 to 12 km), due to smaller sample size in these altitude and SZA intervals.

4.2. TTL: Fresh Convective Outflows and a Stagnant Anticyclone

Convective lifting is thought to be crucial for PGI, as it carries air from lower altitudes to the upper TFT and TTL, redistributing Br-containing species in the troposphere. In addition, an aged plume can allow Br_y to be produced from the decomposition of CBr_y^{VSL} precursors. Here we examine two fresh convective outflows and an aged anticyclone in the TTL and look for enhanced Br_y in these air masses. The convective outflows and the aged anticyclone were identified and located prior to each RF with dynamic models, and confirmed by in situ measured trace gases in-flight.

In RF11 (13 February) between 12 and 14 km we targeted fresh convective outflow originating from a clean MBL (Figure 5). The convective outflow was clearly characterized by high cloud particle concentrations (average 11.8 L^{-1}) and high water-ice content (average 1.3×10^{-3} g · m^{-3}). Low O_3 (27.3 ± 2.2 ppbv, average ± 1σ, sic passim) as well as background levels of CO (95.5 ± 6.8 ppbv) and HCN (144 ± 18 pptv) were consistent with an origin of the clean MBL. Inside the outflow, we observed 0.03 ± 0.26 pptv of BrO (median 0.00 pptv), and 0.003 ± 0.42 pptv of $HOBr + Br_2$, (median 0.00 pptv). We did not find significant BrO or $HOBr + Br_2$ inside this convective plume. Significant levels of BrO and $HOBr + Br_2$ sampled during 00:30 to 01:00 UTC were not of convective origin (see section 4.3).

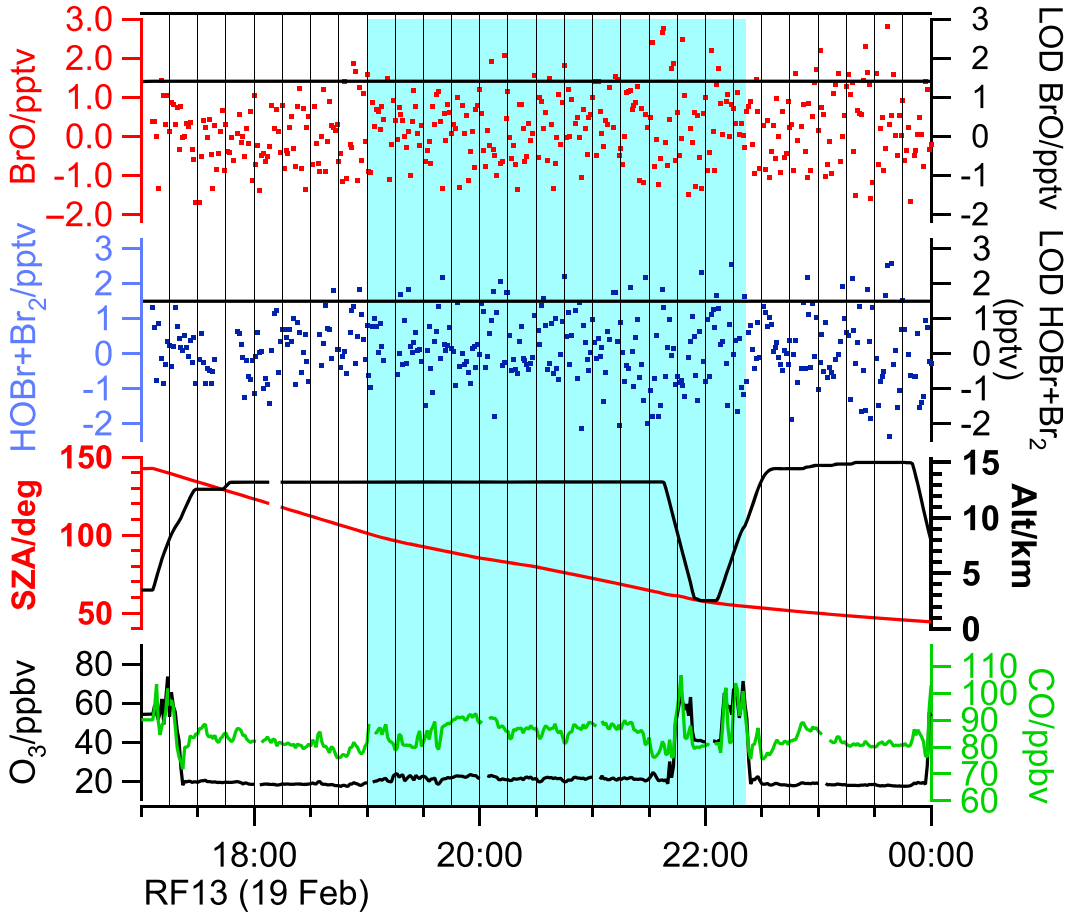

Figure 6. Time series of BrO, HOBr + Br_2, and related species and parameters during RF13. The anticyclone region is shaded in light blue.

Similar results were found for the convective outflow sampled in RF12 (17 February) located between 12 and 14 km to the south and southeast of Guam (Figure 5). This outflow can also be recognized by high water-ice content (average 1.8×10^{-3} g · m^{-3}) and upward motion of air (vertical wind speed, *W*, up to ~1 m · s^{-1}). The cloud particle concentration is unavailable for this flight; but low O_3 (23.5 ± 2.9 ppbv), background levels of CO (79.2 ± 3.2 ppbv) and HCN (112 ± 18 pptv) inside the outflow are consistent with an origin from the unpolluted MBL air. In the plume, BrO was −0.005 ± 0.28 pptv (median 0.025 pptv), and HOBr + Br_2 was 0.19 ± 0.55 pptv (median 0.105 pptv). In the adjacent air masses outside the plume (00:30 to 01:16, 04:07 to 05:00 UTC), we observed −0.04 ± 0.32 pptv of BrO (median −0.02 pptv), and 0.09 ± 0.62 pptv of HOBr + Br_2 (median 0.07 pptv). We did not observe significant levels of BrO or HOBr + Br_2 inside or outside the convective outflow.

A stagnant anticyclone centered at ~12°N, 160°E was probed in RF13 (19 February) before and after sunrise (Figure 6). The GV sampled inside the anticyclone between 19:00 and 22:20 UTC (local sunrise ~19:40 UTC). The GV stayed inside the anticyclone at ~13 km until ~21:40 UTC, then sampled a vertical profile from ~13 km down to ~2.5 km, then flew up to ~14 km. Although different levels of O_3 and CO were observed at different altitudes, no significant BrO or HOBr + Br_2 was observed at any altitude level, inside and outside the anticyclone, prior to and post sunrise.

4.3. Enhanced BrO and/or HOBr + Br_2 in the Tropical-Free Troposphere

Plumes of significant BrO and/or HOBr + Br_2 were episodically observed in the TFT (Table 5). For convenience, we name these plumes with a prefix "Br" and a number (e.g., Br-1). Although our LODs varied with time, in all these plumes, BrO and/or HOBr + Br_2 were clearly elevated. These plumes all featured high O_3, HCN, and

Table 5. Significant BrO and HOBr + Br_2 Levels Observed in the TFT

Plume	RF	Highest BrO (LOD)/pptv[a]	Highest HOBr + Br_2 (LOD)/pptv[a]
Br-1	RF09	2.7 (1.3)	<LOD (3.5)
Br-2	RF09	4.4 (1.3)	<LOD (3.5)
Br-3	RF09	4.5 (1.3)	<LOD (3.5)
Br-4	RF10	6.6 (1.1)	7.3 (3.0)
Br-5	RF11	1.5 (0.6)	3.9 (1.5)
Br-6	RF11	1.0 (0.6)	2.3 (1.5)

[a]Values quoted are flight-averaged LOD.

CH_3CN levels and low relative humidity (RH) (Figure 7). O_3 in these plumes reached 60 to 90 ppbv, in contrast to the typical levels of 20 to 40 ppbv in the TFT. HCN in these plumes ranged from 200 pptv to 468 pptv, compared to background levels of 100 to 150 pptv. RH inside these plumes was generally <10%, except that in plume Br-2 RH varied from 8% to 75% and was probably influenced by mixing processes. In addition, in five out of the six plumes CO was clearly enhanced from the background levels. Finally, CH_3CN was moderately enhanced in all these plumes. Both HCN and CH_3CN are specific tracers of biomass burning emissions [e.g., *Holzinger et al.*, 1999]. All of these plumes are characteristic of the high-ozone, low-water structures that *Anderson et al.* [2016] linked to biomass burning. Particularly, plume Br-4 was an interesting case known as the "CO River," where biomass burning-influenced air was trapped along the subtropical jet [*Pan et al.*, 2016].

The steady state model was applied to check if observed BrO and HOBr + Br_2 levels in these plumes were self-consistent. HOBr + Br_2 was calculated with constraints of observed BrO and other measurements. In three out

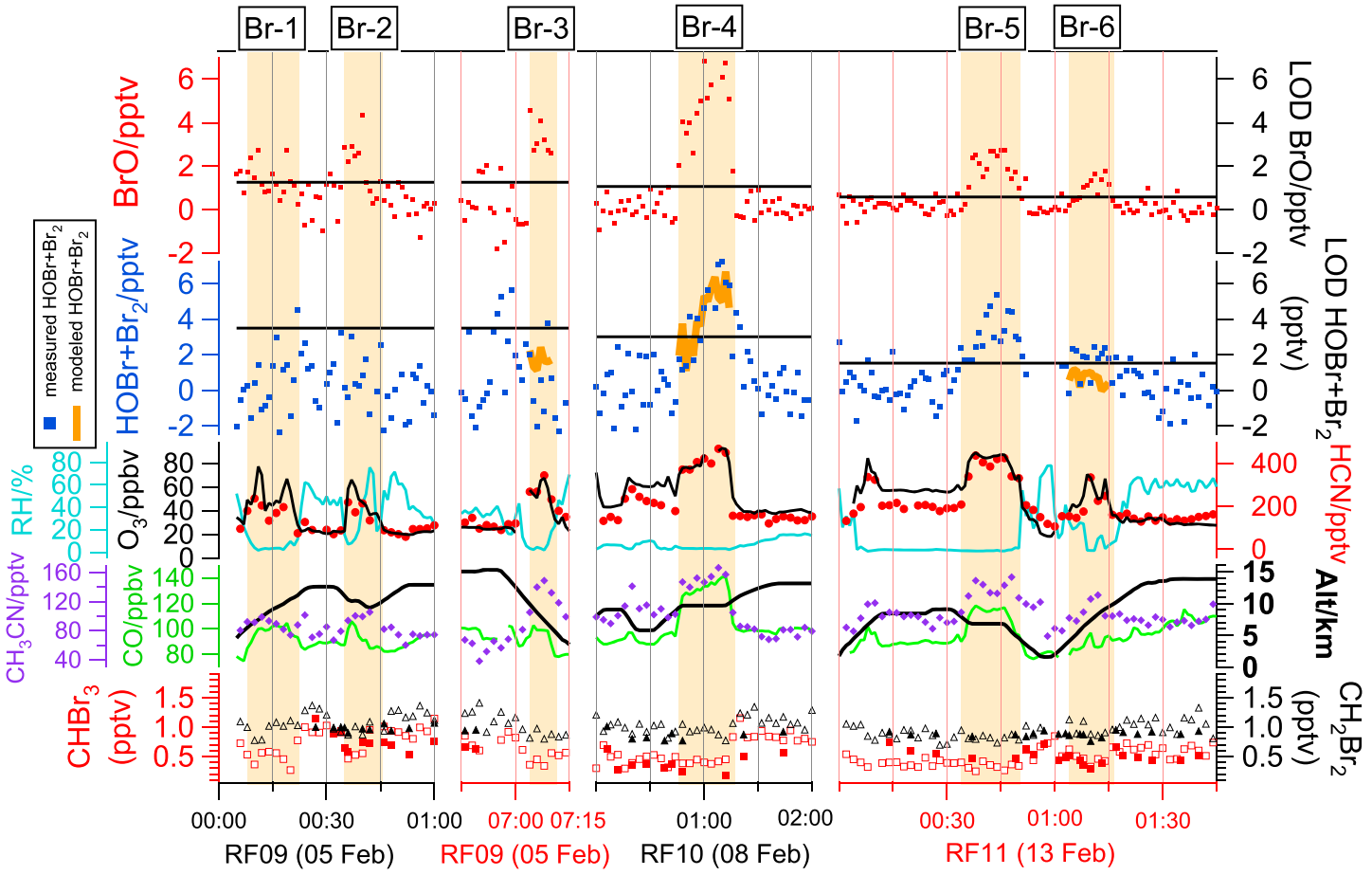

Figure 7. Episodic significant BrO, HOBr + Br_2 in the TFT, and related species and parameters. Plumes of significant BrO and/or HOBr + Br_2 are shaded in light orange. In three of these plumes we had sufficient data to calculate HOBr + Br_2 with the steady state model, using measured BrO as a constraint. Measured HOBr + Br_2 (blue squares) and calculated HOBr + Br_2 (brown solid line) are compared. $CHBr_3$ and CH_2Br_2 measured by AWAS (solid markers) and TOGA (open markers) are also plotted.

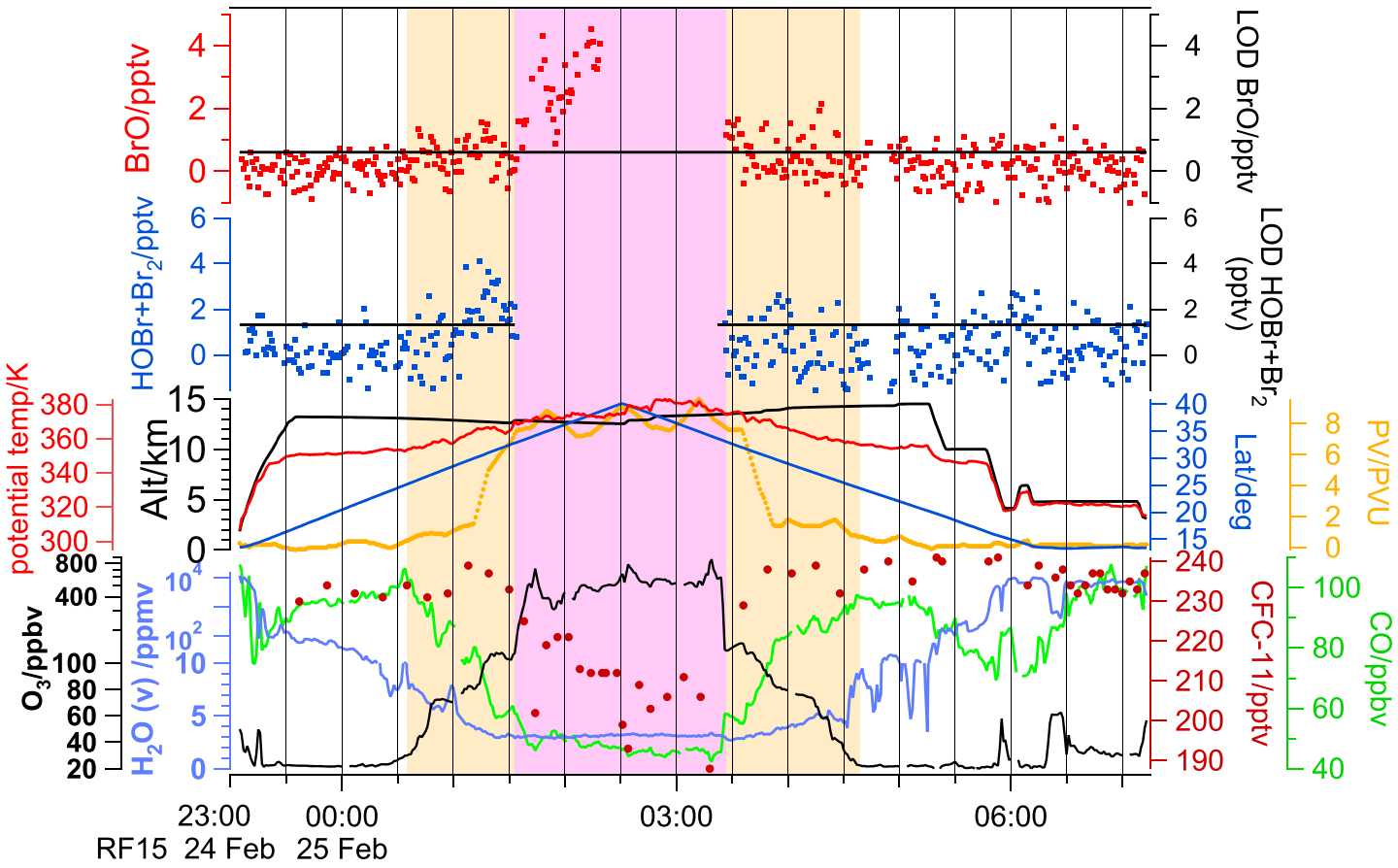

Figure 8. Time series of BrO, HOBr + Br_2, and related species/parameters during RF15. The LMS leg is highlighted in pink, and the TTL-LMS transition region is highlighted in light gold. Note: because of interferences, BrO data are unavailable when O_3 > ~480 ppbv, and HOBr + Br_2 data are unavailable when O_3 > ~125 ppbv.

of the six plumes we had sufficient data to calculate HOBr + Br_2. In all three plumes, the calculated HOBr + Br_2 is consistent with our measured values (Figure 7).

Significant BrO and HOBr in biomass burning plumes has been reported [*Pommier et al.*, 2012]. However, to sustain these amounts of BrO and/or HOBr + Br_2, a strong source of Br_y must be present [*Pommier et al.*, 2012]. Measured $CHBr_3$ and CH_2Br_2 appeared to be slightly lower inside these plumes compared to adjacent air masses. The degradation of $CHBr_3$ and CH_2Br_2 after injection by biomass burning could be a source of Br_y. We do expect bromocarbons to be elevated in biomass plumes in the immediate vicinity of the combustion [e.g., *Simpson et al.*, 2011]. Biomass burning plumes observed over the remote Tropical West Pacific have remained intact, unaffected by recent convective precipitation, for much longer periods of time than adjacent air masses [*Anderson et al.*, 2016]. Therefore, the abundance of $CHBr_3$ and CH_2Br_2 could appear to be suppressed in these biomass burning air masses, relative to adjacent air, due to the longer time for photochemical loss. Since we do not know the original plume concentrations of $CHBr_3$ and CH_2Br_2, this mechanism cannot be further evaluated.

4.4. A Survey From the TTL to the Extratropical LMS

During RF15 (25 February) the GV sampled both the TTL and the extratropical LMS at altitudes of 12 to 14 km, with the northernmost point at ~40°N (see Figure 3 for flight path). Time series of BrO, HOBr + Br_2, and other species/parameters are plotted in Figure 8, together with the potential vorticity (PV). Here the PV was calculated from 6-hourly 1° latitude × 1° longitude, 26 vertical level National Centers for Environmental Prediction Global Forecast System-final (GFS-FNL) analyses and then colocated with GV observations by interpolating in space (latitude, longitude, and pressure) and time along the GV track (http://www.emc.ncep.noaa.gov/gmb/

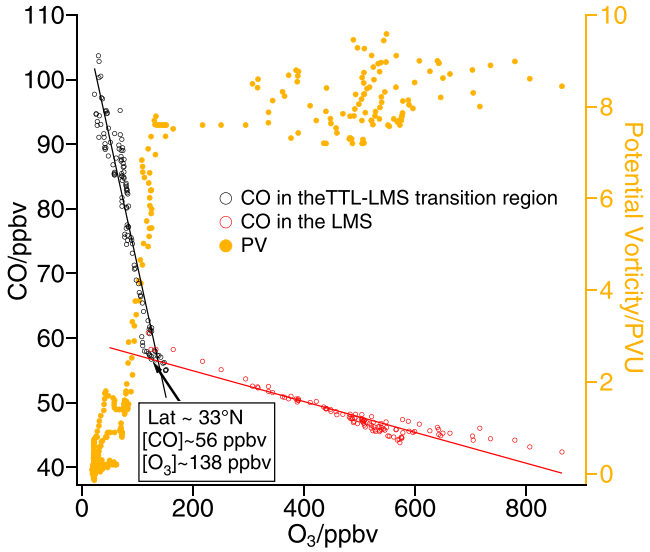

Figure 9. Correlation between CO and O_3 in the TTL-LMS transition region (open black circles) and the LMS (open red circles). In the TTL-LMS transition region, [CO]/ppbv = 110.8 − 0.395 × [O_3]/ppbv ($r = -0.952$). In the LMS, [CO]/ppbv = 59.7 − 0.0239 × [O_3]/ppbv ($r = -0.933$). The CO-O_3 correlations were different in the TTL-LMS transition region and the LMS. The potential vorticity (PV) (solid yellow circles) rapidly increased in the TTL-LMS transition region but was relatively stable in the LMS.

para/parabout.html). A previous application example of the derived PV can be found in *Pan et al.* [2007]. Both chemical tracers and PV clearly displayed the sharp change in the transition from the TTL to the extratropical LMS (Figure 8). In the TTL, O_3, CO, and CFC-11 (CCl_3F) were roughly 20 ppbv, 100 ppbv, and 235 pptv, respectively, and PV was consistently < 1.7 potential vorticity unit (PVU) (1 PVU = $10^{-6}\,K \cdot m^2 \cdot kg^{-1} \cdot s^{-1}$). At latitudes greater than ~25°N, O_3 increased, and CO decreased. Meanwhile, H_2O vapor dropped to < 10 ppmv, and PV rapidly increased from roughly 1.4 PVU to roughly 7.5 PVU. However, CFC-11 still remained at ~235 pptv until ~ 33°N. At ~ 33°N CFC-11 sharply dropped to ~215 pptv, while O_3 sharply increased from ~100 ppbv up to ~800 ppbv. H_2O vapor decreased to 3 to 4 ppmv. PV remained at ~8 PVU. Although O_3 started to increase and CO started to decrease at ~25°N, $\Delta CO/\Delta O_3$ was −0.395 between ~25°N and ~33°N and −0.0239 between ~33°N and ~40°N. At latitudes greater than ~33°N, the sharp increase of O_3, the decrease of CFC-11, plus the high PV values undoubtedly denoted the extratropical LMS. The region between ~25°N and ~33°N should be regarded as a transition region between the TTL and extratropical LMS. In this transition region, CFC-11 levels were the same as in the TTL (~235 pptv), but PV and the CO-O_3 correlation [e.g., *Pan et al.*, 2004] still distinguished it from the LMS and TTL (Figure 9). The discontinuity in CO-O_3 relationship occurred at latitude ~33°N, CO ~56 ppbv, O_3 ~ 138 ppbv, and PV ~6 to 8 PVU. It clearly marked the point of entering the stratosphere. The 6 to 8 PVU PV value near the discontinuity point is very consistent with the climatological PV value that represents the dynamical tropopause at the 370–380 K isentropic level during the Northern Hemisphere winter [*Kunz et al.*, 2011].

We observed different levels of BrO and HOBr + Br_2 in the TTL, the TTL extratropical LMS transition region, and the extratropical LMS. In the TTL, we observed 0.11 ± 0.35 pptv of BrO (median 0.10 pptv), and 0.17 ± 0.64 pptv of HOBr + Br_2 (median 0.10 pptv). In the transition region, we observed 0.48 ± 0.58 pptv of BrO (median 0.34 pptv), and 0.63 ± 1.14 pptv of HOBr + Br_2 (median 0.58 pptv). In the LMS, BrO levels were clearly above zero, up to roughly 4.5 pptv at 480 ppbv of O_3. This survey indicates that BrO and HOBr + Br_2 were near zero in the TTL and started to increase in the TTL-LMS transition region.

5. Discussion

5.1. Br_y Partitioning in the TFT and TTL

The partitioning of Br_y in the TFT and TTL was estimated in two steps. First, photoreactive Br_y was estimated with the steady state model. A constant level of 1 pptv of BrO was assumed for these calculations as this was

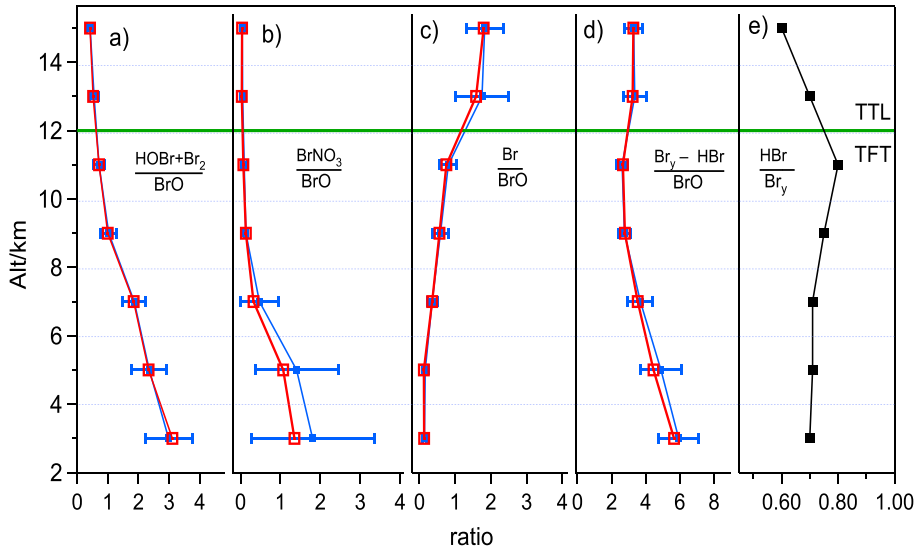

Figure 10. (a–d) Vertical profiles of ([HOBr] + [Br_2])/[BrO], [$BrNO_3$]/[BrO], [Br]/[BrO], and ([Br_y] − [HBr])/[BrO] ratios while SZA < 80°, estimated by the steady state model. The 2 km averages with standard deviations are shown in blue, and 2 km medians are shown in red. (e) Daytime vertical profile of [HBr]/[Br_y] ratio estimated by the time-dependent model.

our approximate LOD for BrO for most of the campaign. For the steady state model we only consider daytime chemistry and thus only use those data points with SZA < 80°, since the steady state assumption does not hold if photodissociation rates are low. After that, HBr was estimated with the time-dependent model. The time-dependent model was run until stable diurnal profiles of Br_y were reached, and thus, the estimated HBr must be regarded as a regional average. We took daytime averages of HBr for comparisons with other Br species. We estimate the daytime vertical profiles of ([HOBr] + [Br_2])/[BrO], [$BrNO_3$]/]BrO], [Br]/[BrO], ([Br_y] − [HBr])/[BrO], and [HBr]/[Br_y], as shown in Figure 10. Given both gas-phase and heterogeneous sources of BrCl ((R8c), (R22), and (R23)), BrCl was still found to be negligible (on the order of 10^{-3} pptv) in the daytime due to its rapid photo dissociation (j(BrCl) ~10^{-2} s^{-1}).

For the daytime photoreactive Br_y budget HOBr was the dominant species from the bottom of the TFT to ~8 km, where ([HOBr] + [Br_2])/[BrO] ranged from 1 to 4 (Figure 10). Yet we did not observe significant HOBr + Br_2, indicating very low BrO in these altitude levels. The ratio of [Br]/[BrO] increased with altitude and is significantly greater than 1 in the TTL, making Br atom the dominant daytime photoreactive Br_y component from ~11 km to the highest altitude we sampled (~15 km). HBr was the major component of Br_y throughout the TFT, accounting for ~70% of Br_y (Figure 10). The dominance of HBr is driven by (1) low O_3, which favors Br atom rather than BrO, and (2) sufficient CH_2O, which reacts with Br atoms to form HBr. BrO was not the dominant Br_y species nor even the dominant photoreactive Br_y species. In the TTL at ~14 km HBr/Br_y dropped to 60%, mostly due to the heterogeneous cycling of HBr ((R21) and (R22)). However, as the ice particle distribution is highly variable in the TTL, our calculation of HBr/Br_y there is uncertain, although it is difficult to estimate the uncertainty based on our data set and model scheme. Consequently, it is possible that HBr/Br_y was less than what we estimated, and Br atoms dominate the bromine distribution in the TTL.

Our findings do not support significant "excess" BrO in the TFT [e.g., *Wang et al.*, 2015], in good agreement with the observation by *Dorf et al.* [2008] and modeling studies by *von Glasow et al.* [2004], *Yang et al.* [2005], *Parrella et al.* [2012], *Liang et al.* [2014], and *Fernandez et al.* [2014]. However, it should be pointed out that low and nearly insignificant levels of BrO and HOBr + Br_2 do not necessarily indicate insignificant Br_y. Indeed, our analysis suggests that HBr is the most abundant Br_y species in the TFT, and either HBr or Br is the most abundant Br_y species in the TTL up to ~15 km. However, HBr and Br atom levels are not constrained by observations, and measurement of these species is needed in future studies.

5.2. Estimation of PGI of Bromine Species

We estimated the amount of PGI of bromine species based on RF15 data. The Br_y profiles from the TTL-LMS transition region to the LMS were inferred with similar processes as in section 5.1. Since CH_2O was well

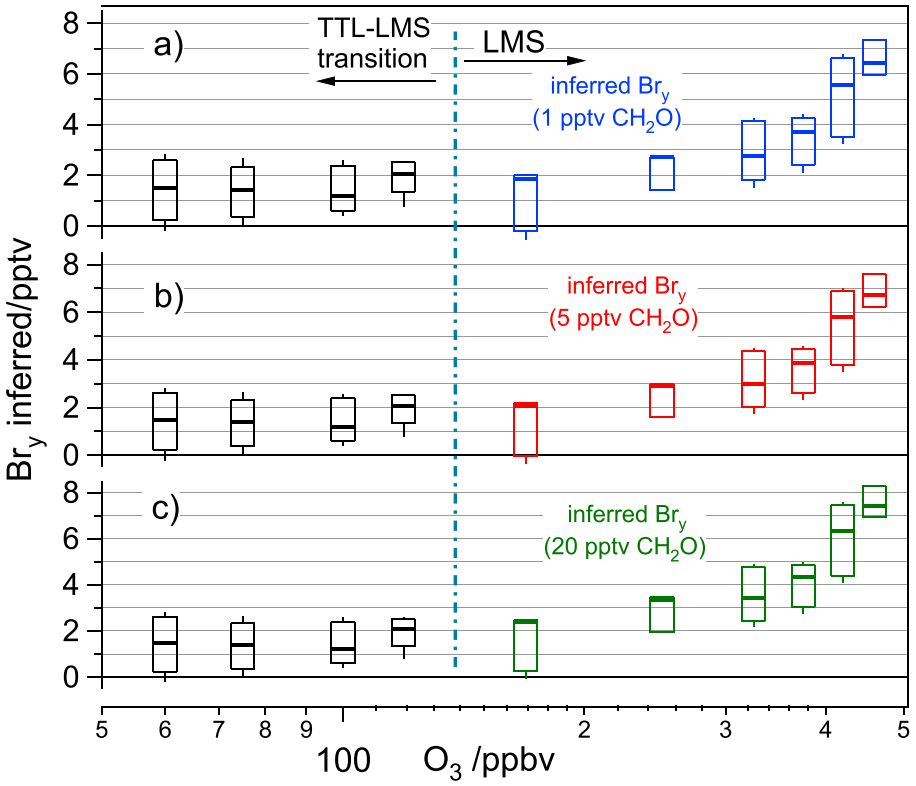

Figure 11. Box and whisker plot of inferred Br_y from the TTL-LMS transition region to the LMS. The bottom and top of the boxes are the first and third quartiles, and the bands inside the box are the medians. The ends of whiskers represent the 10th and 90th percentiles. Br_y in the TTL-LMS transition region was inferred based on measured CH_2O and are plotted in all panels. Br_y in LMS was inferred assuming (a) 1 pptv, (b) 5 pptv, and (c) 20 pptv CH_2O. The boundary between the Q15 TTL-LMS transition region and the LMS is marked.

constrained in the TTL-LMS transition region but not in the LMS, we constrained our models with measured CH_2O in the TTL-LMS transition region but assumed levels of CH_2O (1 pptv, 5 pptv, and 20 pptv) in the LMS leg. However, HBr was found much less sensitive to CH_2O in the LMS than in the TTL/TFT, since partitioning to BrO is favored at high O_3, which suppresses the reaction of Br with CH_2O. The inferred Br_y profiles were plotted against O_3 in Figure 11. We use O_3 as the independent variable, because O_3 is an effective marker of the depth of stratospheric penetration. The inferred Br_y was about 1 to 2 pptv in the TTL-LMS transition region, then slowly increased with increasing O_3. We estimated the PGI of bromine species to be roughly 2 pptv, based on the Br_y level inferred at the boundary between the TTL-LMS transition region and the LMS. This estimate of Br_y is in the range of values recently reported in *Carpenter et al.* [2014] and *Navarro et al.* [2015].

6. Conclusions

We performed observations of BrO and $HOBr + Br_2$ with CIMS during CONTRAST over the Tropical West Pacific. Our observations showed that the levels of BrO and $HOBr + Br_2$ were effectively below our LODs in the TFT and TTL from ~1 km up to ~15.3 km. We did not observe significant levels of BrO and $HOBr + Br_2$ inside multiple fresh deep convective plumes and an aged anticyclone in the TTL. The episodic significant BrO and $HOBr + Br_2$ in the troposphere were found to be associated with elevated O_3, CO, HCN, CH_3CN, and low RH. We postulate these significant Br_y originated from biomass burning. However, the relevant mechanism of the release of Br_y remains unclear. In RF15, profiles of BrO and $HOBr + Br_2$ from the TTL to the extratropical LMS were obtained. In this flight, significant levels of BrO were observed in the extratropical LMS, slightly elevated BrO and $HOBr + Br_2$ were observed in the TTL-LMS transition region, but no significant amount of BrO and $HOBr + Br_2$ was found in the TTL. This is consistent with our findings during other flights that BrO and $HOBr + Br_2$ were near zero in the TTL.

Our observations of BrO gave no indication for excess BrO in the TFT. Furthermore, our analysis of Br_y partitioning shows that during the day HOBr and Br were the dominant photoreactive Br_y species at altitude levels of 1 to 8 km and 11 km to 15 km, respectively. The low levels of $HOBr + Br_2$ we observed from the bottom of the TFT to ~8 km were consistent with even lower BrO. Our analysis also suggests that HBr is the most abundant Br_y species in the TFT, and either HBr or the Br atom is the most abundant Br_y species in the TTL below 15 km. We strongly suggest measuring HBr and Br atoms in future studies. We inferred the Br_y profile from the TTL to the extratropical LMS based on RF15 and estimated PGI of bromine species to be roughly 2 pptv based on the inferred Br_y profiles.

Acknowledgments

D.C., L.G.H., and D.J.T. were supported by the NSF grant 1262033. R.J.S., P.A.W., D.C.A., and JMN received support from the NASA Atmospheric Composition: Modeling and Analysis Program under NNH12ZDA001N-ACMAP and from NSF under grant 1261657. E.A. and V.T. were supported by the NSF AGS grant 1261689. G.M.W., D.C.A., and T.F.H. received support from the NASA Upper Atmospheric Research Program under NNH12ZDA001N-UACO. The authors would like thank the CONTRAST team and the GV crew. CONTRAST data are available online at http://data.eol.ucar.edu/master_list/?project=CONTRAST. CONTRAST data are managed by the Earth Observing Laboratory of the National Center for Atmospheric Research (NCAR/EOL). NCAR is sponsored by the National Science Foundation.

References

Anderson, D. C., et al. (2016), A pervasive role for biomass burning in tropical high ozone/low water structures, *Nat. Commun.*, *7*, 10267, doi:10.1038/ncomms10267.

Arsene, C., A. Bougiatioti, M. Kanakidou, B. Bonsang, and N. Mihalopoulos (2007), Tropospheric OH and Cl levels deduced from non-methane hydrocarbon measurements in a marine site, *Atmos. Chem. Phys.*, *7*, 4661–4673.

Aschmann, J., B.-M. Sinnhuber, E. L. Atlas, and S. Schauffler (2009), Modeling the transport of very short-lived substance into the tropical upper troposphere and lower stratosphere, *Atmos. Chem. Phys.*, *9*, 9237–9247.

Ashfold, M. J., N. R. P. Harris, E. L. Atlas, A. J. Manning, and J. A. Pyle (2012), Transport of short-lived species into the tropical tropopause layer, *Atmos. Chem. Phys.*, *12*, 6309–6322, doi:10.5194/acp-12-6309-2012.

Bertram, T. H., and J. A. Thornton (2009), Toward a general parameterization of N_2O_5 reactivity on aqueous particles: The competing effects of particle liquid water, nitrate and chloride, *Atmos. Chem. Phys.*, *9*, 8351–8363.

Browne, E. C., et al. (2011), Global and regional effects of the photochemistry of $CH_3O_2NO_2$: Evidence from ARCTAS, *Atmos. Chem. Phys.*, *11*, 4209–4219, doi:10.5194/acp-11-4209-2011.

Burkholder, J. B., S. P. Sander, J. Abbatt, J. R. Barker, R. E. Huie, C. E. Kolb, M. J. Kurylo, V. L. Orkin, D. M. Wilmouth, and P. H. Wine (2015), Chemical kinetics and photochemical data for use in atmospheric studies, Evaluation No. 18, JPL Publication 15–10, Jet Propul. Lab., Pasadena. [Available at http://jpldataeval.jpl.nasa.gov.]

Carpenter, L. J., S. Reimann, J. B. Burkholder, C. Clerbaux, B. D. Hall, R. Hossaini, J. C. Laube, and S. A. Yvon-Lewis (2014), Ozone-depleting substances (ODSs) and other gases of interest to the Montreal Protocol, in *Scientific Assessment of Ozone Depletion: 2014*, *Global Ozone Res. and Monit. Proj.-Rep. 55*, chap. 1, World Meteorol. Organ., Geneva, Switzerland.

Choi, S., et al. (2012), Analysis of satellite-derived Arctic tropospheric BrO columns in conjunction with aircraft measurements during ARCTAS and ARCPAC, *Atmos. Chem. Phys.*, *12*, 1255–1285, doi:10.5194/acp-12-1255-2012.

Crowley, J. N., M. Ammann, R. A. Cox, R. G. Hynes, M. E. Jenkin, A. Mellouki, M. J. Rossi, J. Troe, and T. J. Wallington (2010), Evaluated kinetic and photochemical data for atmospheric chemistry: Volume V—Heterogeneous reactions on solid substrates, *Atmos. Chem. Phys.*, *10*, 9059–9223, doi:10.5194/acp-10-9059-2010.

Daniel, J. S., S. Solomon, R. W. Portmann, and R. R. Garcia (1999), Stratospheric ozone destruction: The importance of bromine relative to chlorine, *J. Geophys. Res.*, *104*, 23,871–23,880, doi:10.1029/1999JD900381.

Danilin, M. Y., N.-D. Sze, M. K. W. Ko, J. M. Rodriguez, and M. J. Prather (1996), Bromine-chlorine coupling in the Antarctic ozone hole, *Geophys. Res. Lett.*, *23*, 153–156, doi:10.1029/95GL03783.

Dibb, J. E., L. D. Ziemba, J. Luxford, and P. Beckman (2010), Bromide and other ions in the snow, firn air, and atmospheric boundary layer at Summit during GSHOX, *Atmos. Chem. Phys.*, *10*, 9931–9942.

Dorf, M., A. Butz, C. Camy-Peyret, M. P. Chipperfield, L. Kritten, and K. Pfeilsticker (2008), Bromine in the tropical troposphere and stratosphere as derived from balloon-borne BrO observations, *Atmos. Chem. Phys.*, *8*, 7265–7271.

Fernandez, R. P., R. J. Salawitch, D. E. Kinnison, J.-F. Lamarque, and A. Saiz-Lopez (2014), Bromine partitioning in the tropical tropopause layer: Implications for stratospheric injection, *Atmos. Chem. Phys.*, *14*, 13,391–13,410.

Fitzenberger, R., H. Bösch, C. Camy-Peyret, M. P. Chipperfield, H. Harder, U. Platt, B.-M. Sinnhuber, T. Wagner, and K. Pfeilsticker (2000), First profile measurements of tropospheric BrO, *Geophys. Res. Lett.*, *27*, 2921–2924, doi:10.1029/2000GL011531.

Frieler, K., M. Rex, R. J. Salawitch, T. Canty, M. Streibel, R. M. Stimpfle, K. Pfeilsticker, M. Dorf, D. K. Weisenstein, and S. Godin-Beekmann (2006), Toward a better quantitative understanding of polar stratospheric ozone loss, *Geophys. Res. Lett.*, *33*, L10812, doi:10.1029/2005GL025466.

Hebestreit, K., J. Stutz, D. Rosen, V. Matveiv, M. Peleg, M. Luria, and U. Platt (1999), DOAS measurements of tropospheric bromine oxide in mid-latitudes, *Science*, *283*, 55–57.

Holzinger, R., C. Warneke, A. Hansel, A. Jordan, and W. Lindinger (1999), Biomass burning as a source of formaldehyde, acetaldehyde, methanol, acetone, acetonitrile, and hydrogen cyanide, *Geophys. Res. Lett.*, *26*, 1161–1164, doi:10.1029/1999GL900156.

Hönninger, G., H. Leser, O. Sebastián, and U. Platt (2004), Ground-based measurements of halogen oxides at the Hudson Bay by active long path DOAS and passive MAX-DOAS, *Geophys. Res. Lett.*, *31*, L04111, doi:10.1029/2003GL018982.

Hossaini, R., M. P. Chipperfield, B. M. Monge-Sanz, N. A. D. Richards, E. Atlas, and D. R. Blake (2010), Bromoform and dibromomethane in the tropics: A 3-D model study of chemistry and transport, *Atmos. Chem. Phys.*, *10*, 719–735.

Huey, L. G. (2007), Measurement of trace atmospheric species by chemical ionization mass spectrometry: Speciation of reactive nitrogen and future directions, *Mass Spectrom. Rev.*, *26*, 166–184.

Iraci, L. T., R. R. Michelsen, S. F. M. Ashbourn, T. A. Rammer, and D. M. Golden (2005), Uptake of hypobromous acid (HOBr) by aqueous sulfuric acid solutions: Low-temperature solubility and reaction, *Atmos. Chem. Phys.*, *5*, 1577–1587.

Jacob, D. J. (2000), Heterogeneous chemistry and tropospheric ozone, *Atmos. Environ.*, *34*, 2131–2159.

Kazantseva, N. N., A. Ernepesova, A. Khodjamamedov, O. A. Geldyev, and B. S. Krumgalz (2002), Spectrophotometric analysis of iodide oxidation by chlorine in highly mineralized solutions, *Anal. Chim. Acta*, *456*, 105–119.

Kercher, J. P., T. P. Riedel, and J. A. Thornton (2009), Chlorine activation by N_2O_5: Simulation, in situ detection of $ClNO_2$ and N_2O_5 by chemical ionization mass spectrometry, *Atmos. Meas. Tech.*, *2*, 193–204.

Kim, S., et al. (2007), Measurement of HO_2NO_2 in the free troposphere during the Intercontinental Chemical Transport Experiment–North America 2004, *J. Geophys. Res.*, *112*, D12S01, doi:10.1029/2006JD007676.

Ko, M. K. W., N.-D. Sze, C. J. Scott, and D. K. Wisenstein (1997), On the relation between stratospheric chlorine/bromine loading and short-lived tropospheric source gases, *J. Geophys. Res.*, *102*, 25,507–25,517, doi:10.1029/97JD02431.

Ko, M. K. W., et al. (2002), Very short-lived halogen and sulfur substances, in *Scientific Assessment of Ozone Depletion: 2002*, *Global Ozone Res. and Monit. Proj. – Rep. 47*, chap. 2, Geneva, Switzerland.

Kunz, A., P. Konopka, R. Müller, and L. L. Pan (2011), Dynamical tropopause based on isentropic potential vorticity gradients, *J. Geophys. Res.*, *116*, D01110, doi:10.1029/2010JD014343.

Lee, A. M., R. L. Jones, I. Kilbane-Dawe, and J. A. Pyle (2002), Diagnosing ozone loss in the extratropical lower stratosphere, *J. Geophys. Res.*, *107*(D11), 4110, doi:10.1029/2001JD000538.

Levine, J. G., P. Braesicke, N. R. P. Harris, N. H. Savage, and J. A. Pyle (2007), Pathways and timescales for troposphere-to-stratosphere transport via the tropical tropopause layer and their relevance for very short lived substances, *J. Geophys. Res.*, *112*, D04308, doi:10.1029/2005JD006940.

Liang, Q., E. Atlas, D. Blake, M. Dorf, K. Pfeilsticker, and S. Schauffler (2014), Convective transport of very short lived bromocarbons to the stratosphere, *Atmos. Chem. Phys.*, *14*, 5781–5792, doi:10.5194/acp-14-5781-2014.

Liao, J., et al. (2011a), A comparison of Arctic BrO measurements by chemical ionization mass spectrometry and long path-differential optical absorption spectroscopy, *J. Geophys. Res.*, *116*, D00R02, doi:10.1029/2010JD014788.

Liao, J., et al. (2011b), Observations of inorganic bromine (HOBr, BrO, and Br_2) speciation at Barrow, Alaska, in spring 2009, *J. Geophys. Res.*, *116*, D00R02, doi:10.1029/2011JD016641.

Liao, J., et al. (2012), Characterization of soluble bromide measurements and a case study of BrO observations during ARCTAS, *Atmos. Chem. Phys.*, *12*, 1327–1338, doi:10.5194/acp-12-1327-2012.

Liao, J., et al. (2014), High levels of molecular chlorine in the Arctic atmosphere, *Nat. Geosci.*, *7*, 91–94, doi:10.1038/NGEO2046.

Mahajan, A. S., H. Oetjen, J. D. Lee, A. Saiz-Lopez, G. B. McFiggans, and J. M. C. Plane (2009), High bromine oxide concentrations in the semi-polluted boundary layer, *Atmos. Environ.*, *43*(25), 3811–3818.

Montzka, S. A., et al. (2011), Ozone-depleting substances (ODSs) and related chemicals, in *Scientific Assessment of Ozone Depletion: 2010*, *Global Ozone Res. and Monit. Proj.–Rep. 52*, chap. 1, World Meteorol. Organ., Geneva, Switzerland.

Navarro, M. A., et al. (2015), Airborne measurements of organic bromine compounds in the Pacific tropical tropopause layer, *Proc. Natl. Acad. Sci. U.S.A.*, *112*(45), 13,789–13,793, doi:10.1073/pnas.1511463112.

Neuman, J. A., et al. (2006), Reactive nitrogen transport and photochemistry in urban plumes over the North Atlantic Ocean, *J. Geophys. Res.*, *111*, D23S54, doi:10.1029/2005JD007010.

Neuman, J. A., et al. (2010), Bromine measurements in ozone depleted air over the Arctic Ocean, *Atmos. Chem. Phys.*, *10*, 6503–6514, doi:10.5194/acp-10-6503-2010.

Orlando, J. J. (2003), Atmospheric chemistry of organic bromine and iodine compounds, in *Organic Bromine and Iodine Compounds*, *Handbook of Environmental Chemistry*, vol. 3, Part R, edited by A. H. Nelson, pp. 253–299, Springer, Berlin.

Pan, L. L., W. J. Randel, B. L. Gary, M. J. Mahoney, and E. J. Hintsa (2004), Definition and sharpness of the extratropical tropopause: A trace gas perspective, *J. Geophys. Res.*, *109*, D23103, doi:10.1029/2004JD004982.

Pan, L. L., et al. (2007), Chemical behavior of the tropopause observed during the Stratosphere-Troposphere Analyses of Regional Transport (START) experiment, *J. Geophys. Res.*, *112*, D18110, doi:10.1029/2007JD008645.

Pan, L. L., et al. (2016), The Convective Transport of Active Species in the Tropics (CONTRAST) experiment, *Bull. Am. Meteorol. Soc.*, doi:10.1175/BAMS-D-14-00272.1, in press.

Parrella, J. P., et al. (2012), Tropospheric bromine chemistry: Implications for present and pre-industrial ozone and mercury, *Atmos. Chem. Phys.*, *12*, 6723–6740.

Pommier, M., C. A. McLinden, J. A. Neuman, and J. B. Nowak (2012), Biomass burning in Siberia as a source of BrO to the Arctic free troposphere, *Atmos. Environ.*, *62*, 416–423.

Rudolph, J., B. Ramacher, C. PlassDulmer, K. P. Muller, and R. Koppmann (1997), The indirect determination of chlorine atom concentration in the troposphere from changes in the patterns of non-methane hydrocarbons, *Tellus, Ser. B*, *49*(5), 592–601, doi:10.1034/j.1600-0889.49.issue5.13.x.

Salawitch, R. J. (2006), Biogenic bromine, *Nature*, *439*(19), 275–276.

Salawitch, R. J., et al. (1993), Chemical loss of ozone in the arctic polar vortex in the winter of 1991–1992, *Science*, *261*, 1146–1149.

Salawitch, R. J., D. K. Weisenstein, L. J. Kovalenko, C. E. Sioris, P. O. Wennberg, K. Chance, M. K. W. Ko, and C. A. McLinden (2005), Sensitivity of ozone to bromine in the lower stratosphere, *Geophys. Res. Lett.*, *32*, L05811, doi:10.1029/2004GL021504.

Schofield, R., K. Kreher, B. J. Connor, P. V. Johnston, A. Thomas, D. Shooter, M. P. Chipperfield, C. D. Rodgers, and G. H. Mount (2004), Retrieved tropospheric and stratospheric BrO columns over Lauder, New Zealand, *J. Geophys. Res.*, *109*, D14304, doi:10.1029/2003JD004463.

Schwartz, S. E. (1986), Mass-transport considerations pertinent to aqueous-phase reactions of gases in liquid-water clouds, in *Chemistry of Multiphase Atmospheric Systems*, edited by W. Jaechske, pp. 415–471, Springer, Heidelberg.

Simpson, I. J., et al. (2011), Boreal forest fire emissions in fresh Canadian smoke plumes: C1–C10 volatile organic compounds (VOCs), CO_2, CO, NO_2, NO, HCN and CH_3CN, *Atmos. Chem. Phys.*, *11*, 6445–6463, doi:10.5194/acp-11-6445-2011.

Sinnhuber, B.-M., and I. Folkins (2006), Estimating the contribution of bromoform to stratospheric bromine and its relation to dehydration in the tropical tropopause layer, *Atmos. Chem. Phys.*, *6*, 4755–4761.

Sinnhuber, B.-M., A. Rozanov, N. Sheode, O. T. Afe, A. Richter, M. Sinnhuber, F. Wittrock, and J. P. Burrows (2005), Global observations of stratospheric bromine monoxide from SCIAMACHY, *Geophys. Res. Lett.*, *32*, L20810, doi:10.1029/2005GL023839.

Sioris, C. E., et al. (2006), Latitudinal and vertical distribution of bromine monoxide in the lower stratosphere from Scanning Imaging Absorption Spectrometer for Atmospheric Chartography limb scattering measurements, *J. Geophys. Res.*, *111*, D14301, doi:10.1029/2005JD006479.

Sjostedt, S. J., et al. (2007), Observations of hydroxyl and the sum of peroxy radicals at Summit, Greenland during summer 2003, *Atmos. Environ.*, *41*, 5122–5137.

Slusher, D. L., L. G. Huey, D. J. Tanner, F. M. Flocke, and J. M. Roberts (2004), A thermal dissociation-chemical ionization mass spectrometry (TD-CIMS) technique for the simultaneous measurement of peroxyacyl nitrates and dinitrogen pentoxide, *J. Geophys. Res.*, *109*, D19315, doi:10.1029/2004JD004670.

Tegtmeier, S., K. Krüger, B. Quack, E. L. Atlas, I. Pisso, A. Stohl, and X. Yang (2012), Emission and transport of bromocarbons: From the West Pacific Ocean into the stratosphere, *Atmos. Chem. Phys.*, *12*, 10,633–10,648.

Theys, N., M. V. Roozendael, F. Hendrick, C. Fayt, C. Hermans, J.-L. Baray, F. Goutail, J.-P. Pommereau, and M. D. Mazière (2007), Retrieval of stratospheric and tropospheric BrO columns from multi-axis DOAS measurements at Réunion Island (21°S, 56°E), *Atmos. Chem. Phys.*, *7*, 4733–4749.

van Roozendael, M., et al. (2002), Intercomparison of BrO measurements from ERS-2 GOME, ground-based and balloon platforms, *Adv. Space Res.*, *29*, 1661–1666.

von Glasow, R., R. von Kuhlmann, M. G. Lawrence, U. Platt, and P. J. Crutzen (2004), Impact of reactive bromine chemistry in the troposphere, *Atmos. Chem. Phys.*, *4*, 2481–2497.

Wang, S., et al. (2015), Active and widespread halogen chemistry in the tropical and subtropical free troposphere, *Proc. Natl. Acad. Sci. U.S.A.*, *112*(30), 9281–9286, doi:10.1073/pnas.1505142112.

Warwick, N. J., A. Pyle, G. D. Carver, X. Yang, N. H. Savage, F. M. O'Connor, and R. A. Cox (2006), Global modeling of biogenic bromocarbons, *J. Geophys. Res.*, *111*, D24305, doi:10.1029/2006JD007264.

Wennberg, P. O., et al. (1994), Removal of stratospheric O_3 by radicals: In situ measurements of OH, HO_2, NO, NO_2, ClO and BrO, *Science*, *266*, 398–404.

Wolfe, G. M., and J. A. Thornton (2011), The Chemistry of Atmosphere-Forest Exchange (CAFE) Model—Part 1: Model description and characterization, *Atmos. Chem. Phys.*, *11*(1), 77–101, doi:10.5194/acp-11-77-2011.

World Meteorological Organization (WMO) (2011), *Scientific Assessment of Ozone Depletion: 2010*, *Global Ozone Res. and Monit. Proj. – Rep. 52*, 516 pp., World Meteorol. Organ., Geneva, Switzerland.

World Meteorological Organization (WMO) (2014), *Scientific Assessment of Ozone Depletion: 2014*, *Global Ozone Res. and Monit. Proj.– Rep. 55*, 416 pp., World Meteorol. Organ., Geneva, Switzerland.

Wu, C.-H., M. M. Birky, and L. G. Hepler (1963), Thermochemistry of some bromine and iodine species in aqueous solution, *J. Phys. Chem.*, *67*(6), 1202–1205, doi:10.1021/j100800a009.

Yang, X., R. A. Cox, N. J. Warwick, J. A. Pyle, G. D. Carver, F. M. O'Connor, and N. H. Savage (2005), Tropospheric bromine chemistry and its impacts on ozone: A model study, *J. Geophys. Res.*, *110*, D23311, doi:10.1029/2005JD006244.

Zheng, W., F. M. Flocke, G. S. Tyndall, A. Swanson, J. J. Orlando, J. M. Roberts, L. G. Huey, and D. J. Tanner (2011), Characterization of a thermal decomposition chemical ionization mass spectrometer for the measurement of peroxy acyl nitrates (PANs) in the atmosphere, *Atmos. Chem. Phys.*, *11*, 6529–6547, doi:10.5194/acp-11-6529-2011.